

Politecnico di Torino

Master's degree in Mathematical Engineering



Cancer cells phenotype evolution in hypoxic conditions.

Professors

Chiara Giverso
Luigi Preziosi
Luca Mesin

Candidates

Biagio Torsello ([LinkedIn profile](#))
Francesca Marino ([LinkedIn profile](#))
Ludovica D'Incà ([LinkedIn profile](#))

Academic Year 2023-2024

Contents

1	Introduction	3
1.1	The biological problem	3
1.1.1	Stages of tumor growth	3
1.1.2	Tumor as a complex evolving system	3
1.2	Phenotypic heterogeneity in vascularized tumours	4
1.2.1	The role of intratumoral oxygen concentration	4
1.2.2	Biomedical needs and application in cancer therapy	4
1.3	Models in literature	5
2	Methods	5
2.1	Cancer cells dynamic	5
2.1.1	Energy (ATP) balance	6
2.1.2	Cellular proliferation and death	7
2.1.3	Transport in the physical space	8
2.1.4	Transport in the phenotypic space	8
2.1.5	Boundary conditions and initial conditions	8
2.2	Glucose and oxygen dynamic	9
2.2.1	Boundary conditions and initial conditions	10
2.3	Qualitative analysis	10
2.4	Case study: only spontaneous phenotype changes	13
2.4.1	Fitness function G	14
3	Numerical Simulations	14
3.1	Mono-dimensional scenario	15
3.2	Bi-dimensional scenario	17
3.3	Case study: spontaneous phenotype changes only	18
4	Results	19
4.1	Mono-dimensional case	19
4.2	Bi-dimensional case	21
4.2.1	One vessel - Gaussian and uniform initial condition	21
4.2.2	Three vessels - uniform initial condition	23
5	Conclusions	25
5.1	On future research	25
I	Michaelis-Menten equations	26

1 Introduction

1.1 The biological problem

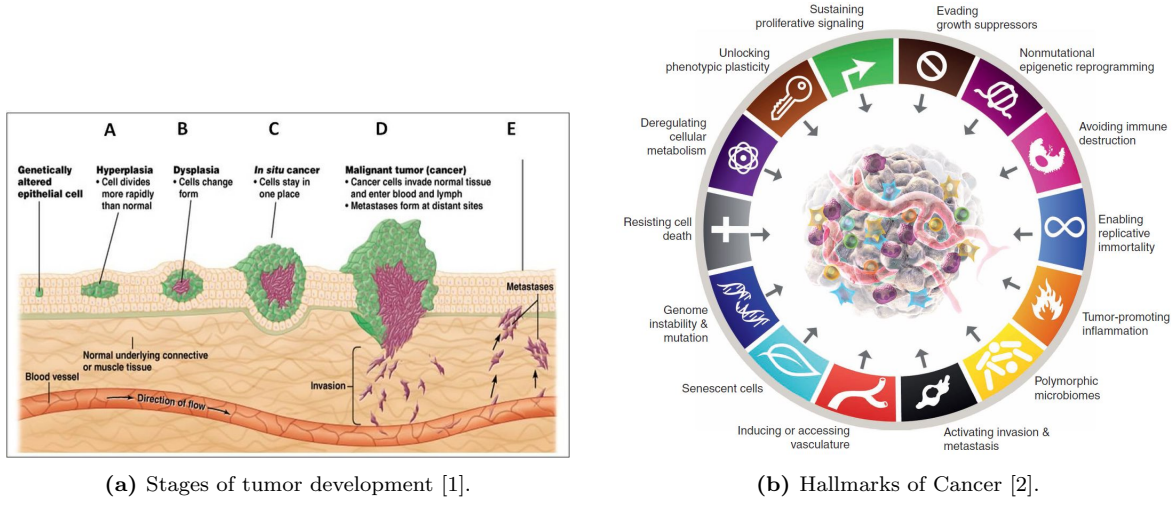


Figure 1

1.1.1 Stages of tumor growth

Cancer is a constantly evolving dynamic disease which leads to genotypic and phenotypic changes of properties in cancer cells across space and time within the same tumour. Moreover, the dynamic of tumours with the same histological features is likely to vary across patients [3].

The development of cancer starts when some cells within a healthy population undergo genetic mutations that increase their propensity to proliferate (Figure 1a) due to the loss of homeostasis, so the cells can not detect what happens in the surrounding micro-environment. The altered cells and their descendants will continue to look normal for a certain amount of time, reproducing however at a higher rate, which at the end results in having a high number of modified cells (**hyperplasia**). After years, one in a million of these modified cells suffer another mutation that causes further loss of control on cell growth. In addition to the excessive proliferation a new genetic mutation can occur so that cells change morphology and appear abnormal in both shape and orientation (**dysplasia**).

After all these changes, cancer cells can not be controlled anymore and even if during the first phases tumor cells do not break into any boundaries between tissues (this phase *in situ* is called **avascular growth phase**), there could be a moment in time when growing cells will provoke the development of new blood vessel¹ (**vascular growth phase**) and will seep through them, spreading throughout the body (*invasion* and *metastasis*).

Even if cancer is characterized by extreme heterogeneity, it is possible to find some common fundamental characteristics between the many different kinds. In particular, D. Hanahan and R. Weinberg provided a conceptual framework that rationalizes the complexity of different tumor types in terms of a common set of underlying cellular parameters ([4], [5], [2]); their results are summarized in Figure 1b.

1.1.2 Tumor as a complex evolving system

Different studies emphasize how tumors can be described as spatially and temporally heterogeneous systems that continually adapt to the micro-environment in order to evolve by increasing the fitness of cancer cells ([6], [4]). On the other hand, cancer cells are also able to modify the surrounding micro-environment, as previously mentioned, to make it more suitable for tumor growth and expansion. This interplay between the ability of cancer cell to modify the surrounding environment and the

¹The transition of tumor growth from the avascular to the vascular phase is accomplished throughout the secretion of TAFs (Tumor Angiogenic Factors) into the surrounding tissues which stimulate the production of endothelial cells, leading to the formation of new blood vessels that will supply the tumor with oxygen and essential nutrients.

micro-environment itself can lead to intratumoral heterogeneity, i.e. selection of different phenotypic characteristics ([6]). In particular, the gradual appearance of phenotypic heterogeneity in vascularized tumours is the result of a process driven by the spatial variability of abiotic components in the micro-environment: among all of them, oxygen is one of the key factors ([7]).

1.2 Phenotypic heterogeneity in vascularized tumours

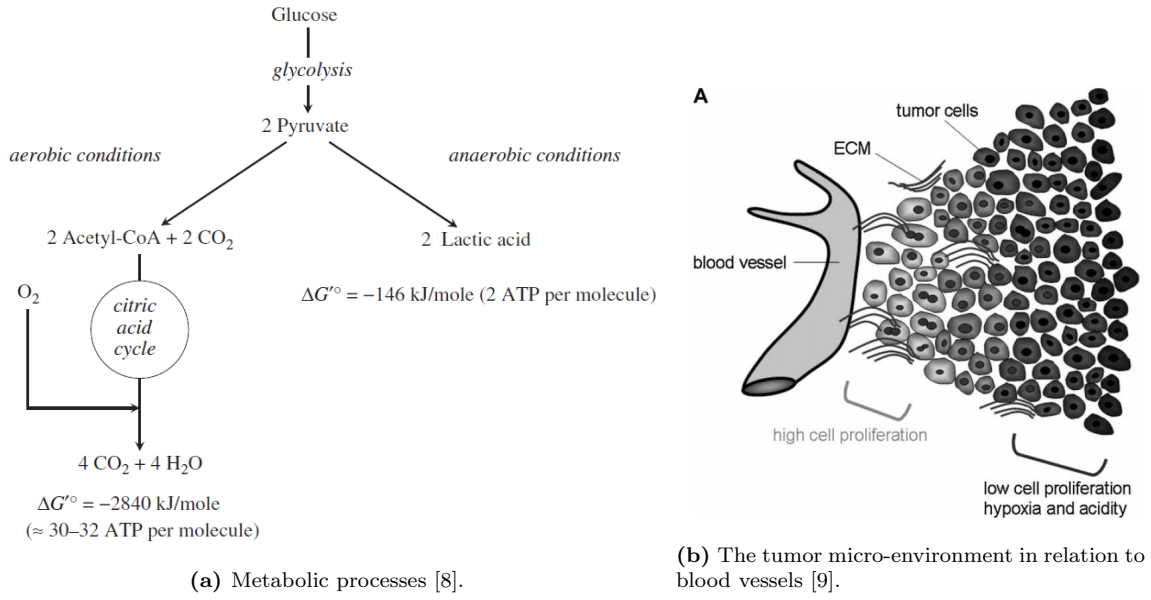


Figure 2

1.2.1 The role of intratumoral oxygen concentration

Metabolic processes within healthy tissues require oxygen: six molecules of oxygen are consumed per oxidized molecule of glucose with the yield of approximately 32 molecules of ATP (Figure 2a). In many intense cancers proliferation the lack of available oxygen supply leads to hypoxia (Figure 2b). In such conditions (i.e. when oxygen levels are below physiological ones) cells may rely on glycolysis only, the first step of glucose oxidation, in order to cover their energy needs; the latter produces a smaller amount of ATP: 2 molecules of ATP are produced per molecule of glucose (Figure 2a). As a matter of fact most tumours are known to rely on glycolytic metabolism even in non-hypoxic conditions². In this instance, lactic acid produced by cancer cells in the glycolytic metabolism increases the acidity levels of the micro-environment becoming more suitable for tumor survival and proliferation ([3]). It follows that intratumoral oxygen concentration is a fundamental factor, as mentioned in section 1.1.2, for the evolutionary dynamic of cancer cells in vascularized tumors. Experimental and clinical studies have demonstrated that well-oxygenated regions are mainly populated by cells characterized by low levels of **hypoxia-inducible factors** (e.g. HIF-1 α)³, whereas hypoxic tumor regions are constituted by slow-dividing cells with high levels of these factors.

1.2.2 Biomedical needs and application in cancer therapy

The crucial role given by the interplay between cancer cells and micro-environment has led to a new definition of tumor as a “*complex adaptive system*” ([10]). This new theoretical framework can be a starting point for innovative cancer therapies: *ecological therapy* ([6]), for example, aims at targeting not only tumors but also its micro-environment and their interactions. In particular, several studies have highlighted the value of understanding the phenotypic evolution of tumor cells to hypoxic micro-environments for the development of effective therapies ([11]). Mathematical modelling can

²This effect is known as **Warburg effect** or aerobic glycolysis, and is one of the hallmarks of cancer [8] (Figure 1b).

³HIF is a fundamental protein in the cell metabolism that plays the role of indicator of the level of hypoxia, i.e. it is a sensor of the quantity of oxygen present in the cell and in the surrounding environment.

be an important tool for contextualizing empirical evidences in a more rigorous framework and for predicting possible emergent phenomena.

1.3 Models in literature

The aim of the work is to describe the transition of tumor cells from an aerobic to an anaerobic metabolism and the switch is assumed to happen in hypoxic conditions. Moreover two different domain will be taken into account: firstly the uni-dimensional one (in space) will be studied and then the research will move on to the bi-dimensional scenario (in space) with different settings and blood vessels configurations.

Many other works have tried to give an explanation for this phenomenon, with many different mathematical approaches. As previously mentioned, the shift towards glycolitic metabolism is often irreversible in tumors and even if there is a sufficient quantity of oxygen, cells might keep an anaerobic metabolism. For this reason the current work takes into account two distinct cell lines with different metabolic behaviour: the first one is related to cells whose metabolism requires oxygen which will be called *aerobic* and the second one refers to cells with glycolytic metabolism which will be called *anaerobic* ([8]).

It is worth to cite [3], in which the authors study the influence of hypoxia and acidity on the evolutionary dynamic of a vascularized tumor: the model is a system of non-local partial integro-differential equations that describe the phenotypic evolution of cancer cells in response to variations of oxygen, glucose and lactate. The phenotype is represented by a bi-dimensional variable with normalized level of expression of HIF-1 α gene and acidity resistance gene.

The interplay between tumor cells, oxygen concentration and chemotherapeutic agent concentration is studied in [7], in which it is underlined how hypoxic regions support intra-tumoral heterogeneity and favour the selection of chemoresistant phenotypic variants.

Another important contribution is given by [8], in which the authors used a multiphase approach, as in a porous media mechanic problem: the volume ratio of healthy and cancerous cells had been taken into account, so that the model is a bi-population model with two different domains. Also, in the so said study the Warburg effect takes place in hypoxic conditions and the acid-resistance of glycolytic cells is an important step towards cancer invasiveness.

2 Methods

2.1 Cancer cells dynamic

In the model presented hereafter the cancer cells spatial variable will be denoted as $\mathbf{x} \in \Omega \subset \mathbb{R}^d$, in which $d = 1, 2$ and Ω is the domain describing the considered tissue. The internal variable $h \in [0, 1]$, instead, represents the phenotype of cancer cells which is described by the normalized level of expression of the hypoxia-inducible factor HIF-1 α . It has been previously mentioned that scientific evidence states that areas with lower levels of oxygen are characterised by the presence of cells with higher levels of expression of the factor HIF-1 α whereas regions with physiological levels of oxygen are characterised by the presence of cells with lower levels of expression of the factor HIF-1 α .

Denoting with $\phi_c(t, \mathbf{x}) \in [0, 1]$ the volume fraction of cancer cells, with $\phi_h(t, \mathbf{x}) \in [0, 1]$ the volume fraction of healthy cells and with $\phi_m(t, \mathbf{x}) \in [0, 1]$ the volume fraction of ECM, we can write:

$$\phi_c + \phi_h + \phi_m = \bar{\phi} \leq 1$$

in which $\phi_c, \phi_h, \phi_m \in [0, \bar{\phi}]$.

Writing the volume fraction as

$$\tilde{\phi}_c = \frac{\phi_c}{\bar{\phi}} \quad \tilde{\phi}_h = \frac{\phi_h}{\bar{\phi}} \quad \tilde{\phi}_m = \frac{\phi_m}{\bar{\phi}}$$

we have $\tilde{\phi}_c + \tilde{\phi}_h + \tilde{\phi}_m = 1$.

In this model the tissue in which the dynamic of cancer cells evolves is considered fixed and made up of healthy cells and ECM. This hypothesis allows to simplify the model considering $\phi_c = \phi$.

Lastly, let us denote with $f(t, \mathbf{x}, h)$ the local phenotype distribution of cancer cells in which $t \in [0, T]$

with $T > 0$. At this point, at every time t the volume fraction of cancer cells (1) and the average phenotype distribution (2) can be described as:

$$\phi(t, \mathbf{x}) = \int_0^1 f(t, \mathbf{x}, h) dh \quad (1)$$

$$H(t, \mathbf{x}) = \frac{1}{\phi(t, \mathbf{x})} \int_0^1 h f(t, \mathbf{x}, h) dh \quad (2)$$

The evolution of $f(t, \mathbf{x}, h)$ can be written as:

$$\partial_t f + \underbrace{\nabla_{(\mathbf{x})} \cdot (f \mathbf{v})}_{(1)} + \underbrace{\partial_h(fw)}_{(2)} - \underbrace{\beta \partial_{hh}^2 f}_{(3)} = \underbrace{Gf}_{(4)} \quad (3)$$

In which

$$\mathbf{v} \equiv \mathbf{v}(h, \phi(t, \mathbf{x})) \quad w \equiv w(h, c_o(t, \mathbf{x}), c_g(t, \mathbf{x})) \geq 0$$

Analyzing the partial differential equation (3) we have that:

- (1) represents the transport of cells in the physical space, Ω ;
- (2) represents the transport in the phenotypic space, h ;
- (3) describes the changes in the distribution f due to spontaneous variations of phenotype that take place with rate β ;
- (4) represents the source term;

Moreover, the function G in the source term (4) models the *fitness*, namely the net proliferation rate, that can be thought as the sum of two terms:

- the *effective proliferation*: $(p(\bar{\phi} - \phi))_+$, in which $p \equiv p(h, c_o(t, \mathbf{x}), c_g(t, \mathbf{x}))$;
- the cells death: d , in which $d \equiv d(h, c_o(t, \mathbf{x}), c_g(t, \mathbf{x}))$;

The net proliferation rate is:

$$G = (p(\bar{\phi} - \phi))_+ - d \quad (4)$$

Moreover cancer cells evolve thanks to the availability of oxygen and glucose. It follows that it is necessary to define the concentration of oxygen and glucose inside Ω such as:

$$c_o(t, \mathbf{x}) \quad c_g(t, \mathbf{x})$$

2.1.1 Energy (ATP) balance

As it has been already explained in section 1.2.1, there are two different pathways cells can take in order to produce ATP (described in figure 2a), necessary for the sustenance of the cells. The difference between the two is given by the availability of nutrients (mostly oxygen) in the environment in which cells live:

1. **aerobic conditions** ($h \rightarrow 0$): $\text{Glc} + 6\text{O}_2 \longrightarrow 6\text{CO}_2 + N\text{ATP}$ with N varying from 34 to 38;
2. **anaerobic conditions** ($h \rightarrow 1$): $\text{Glc} \longrightarrow 2\text{Lactic Acid} + 2\text{ATP}$.

As clearly written in the reactions above, the nutrient factor that discerns the two pathways is oxygen. In particular, glycolysis produce 2 ATP molecules and it is a fundamental step in both aerobic and anaerobic cellular respiration.

The non-dimensional ATP quantities produced by the aerobic and anaerobic pathways are defined as q_o^{ATP} and q_g^{ATP} , respectively. The availability of oxygen in the environment is described through a Michaelis-Menten function $a(c_o) \equiv a(c_o(t, \mathbf{x}))$ ⁴:

⁴More information on Michaelis-Menten equation can be found in the appendix, section I.

$$a(c_o) = \frac{c_o}{M_o + c_o} \quad (5)$$

For the same reasons, the function $b(c_g) \equiv b(c_g(t, \mathbf{x}))$ describing the availability of glucose in the environment was also modelled through a Michaelis-Menten type of equation:

$$b(c_g) = \frac{c_g}{M_g + c_g} \quad (6)$$

The non-dimensional ATP quantities produced by the aerobic and anaerobic pathway then become:

$$q_o^{ATP}(c_o(t, \mathbf{x}), c_g(t, \mathbf{x})) = 36a(c_o)b(c_g) \quad q_g^{ATP}(c_g(t, \mathbf{x})) = 2b(c_g)$$

These quantities allow to define a rate of production of ATP as:

$$q_o(c_o(t, \mathbf{x}), c_g(t, \mathbf{x})) = \kappa_o q_o^{ATP} \quad q_g(c_g(t, \mathbf{x})) = \kappa_g q_g^{ATP} \quad (7)$$

in which κ_o and κ_g are rates that describe the speed of the reactions above.

It is important to highlight that even though the anaerobic pathway seems inefficient compared to the aerobic one, the metabolic rate of glucose in anaerobic conditions is higher; in particular, the production of lactate is 10 – 100 times faster than the complete oxidation of glucose.

2.1.2 Cellular proliferation and death

Even though the following hypothesis is far from reality, it is assumed that ATP can not be collected, but it is fully consumed by cells. For sake of simplicity let us also assume that cells use ATP at a rate θ to grow and live and the rest of the energy is used for cell proliferation.

In this paper, in agreement with experimental evidences, it is assumed that cells that are characterized by a higher expression of factor HIF-1 α ($h \rightarrow 1$) are more likely to follow the anaerobic pathway to produce energy, whereas cells with lower values of factor HIF-1 α ($h \rightarrow 0$) are more likely to follow the aerobic pathway. Since, as previously mentioned, proliferation depends on the amount of available energy, it is useful defining the rate of total energy produced by a single cell with phenotype h as a weighted sum:

$$q \equiv q(h, c_o(t, \mathbf{x}), c_g(t, \mathbf{x})) = n_o(h)q_o(c_o(t, \mathbf{x}), c_g(t, \mathbf{x})) + n_g(h)q_g(c_g(t, \mathbf{x})) \quad (8)$$

in which

$$\begin{aligned} n_o(0) &= 1, & n_o(1) &= 0, & n'_o(h) &< 0, & \forall h \in (0, 1) \\ n_g(0) &= 0, & n_g(1) &= 1, & n'_g(h) &> 0, & \forall h \in (0, 1) \end{aligned} \quad (9)$$

From (8) it can be stated that the energy produced by cells depends on both environmental conditions and the level of expression of factor HIF-1 α : the latter, in fact, has a fundamental role on the energetic pathway choice. In this paper the following functions are chosen:

$$n_0(h) = (1 - h)^2, \quad n_g(h) = 1 - (1 - h)^2$$

As a consequence, the rate of total energy is:

$$q = (1 - h)^2 q_o + [1 - (1 - h)^2] q_g \quad (10)$$

which is increasing in both q_o and q_g . Moreover, the non-dimensional rate of total energy normalized with respect to the rate θ necessary for the sustenance and growth of tumor cells is:

$$\tilde{q} := \frac{q}{\theta}$$

Consequently, the function $(\tilde{q} - 1)_+$ determines the available quantity of ATP.⁵

Now, assuming that the previously mentioned proliferation function p is proportional to the ATP available, the so said function can be written as:

$$p(h, c_o(t, \mathbf{x}), c_g(t, \mathbf{x})) = \eta(\tilde{q}(h, c_o(t, \mathbf{x}), c_g(t, \mathbf{x})) - 1)_+ \quad (11)$$

⁵Remark: the definition of the positive part function $((\cdot)_+)$ is:

$$f^+(x) = \max(f(x), 0) = \begin{cases} f(x) & \text{if } f(x) > 0, \\ 0 & \text{otherwise} \end{cases}$$

with η being a scaling factor.

Instead, for what concerns the death term d , we assume that cells death is caused by two different phenomena:

- apoptosis, which takes place with rate ξ ;
- insufficient energy to live, which takes place when $\tilde{q} < 1$

Function d then becomes:

$$d(h, c_o(t, \mathbf{x}), c_g(t, \mathbf{x})) = \xi + \xi_q(1 - \tilde{q}(h, c_o(t, \mathbf{x}), c_g(t, \mathbf{x})))_+ \quad (12)$$

with ξ_q being a scaling factor. With the new definitions of the proliferation function (11) and of the death function (12), it is immediate to re-write the fitness G as:

$$\begin{aligned} G(h, c_o(t, \mathbf{x}), c_g(t, \mathbf{x})) &= \\ (\bar{\phi} - \phi(t, \mathbf{x}))_+ - d &= \\ \eta(\bar{\phi} - \phi(t, \mathbf{x}))_+ (\tilde{q}(h, c_o(t, \mathbf{x}), c_g(t, \mathbf{x})) - 1)_+ - \xi - \xi_q(1 - \tilde{q}(h, c_o(t, \mathbf{x}), c_g(t, \mathbf{x})))_+ & \end{aligned} \quad (13)$$

2.1.3 Transport in the physic space

For what concerns \mathbf{v} (velocity in physic space), it is assumed that cells move through the fixed porous scaffold of the tumor following the opposite direction of the gradient of $\phi(t, \mathbf{x})$. Since some studies have demonstrated that factor HIF-1 α promotes cellular migration, it is assumed that \mathbf{v} depends also on the variable h . The velocity takes the form:

$$\mathbf{v}(h, \phi(t, \mathbf{x})) = -\mu(h)\nabla_{(\mathbf{x})}(\phi(t, \mathbf{x})) \quad (14)$$

in which

$$\mu(0) > 0, \quad \frac{d\mu(h)}{dh} > 0 \quad \forall h \in (0, 1)$$

The latter highlights the fact that higher values of h corresponds to higher values of $\mu(h)$, also known as motility.

2.1.4 Transport in the phenotypic space

In equation (3), which has been already analysed, there is a term describing the transport in the phenotypic variable: $\partial_h(fw)$ in which w represents the rate of the induced phenotype changes, describing the Warburg effect.

It is assumed that phenotype changes happen when the energy production induced by aerobic cellular respiration only is not sufficient for the cell growth and its sustainment; the reason behind this assumption is that gene HIF-1 α accumulate in hypoxic environment. Moreover, the rate w is such that phenotypic changes are not catalytic actions and w should decrease with the increase of oxygen availability.

Another way to describe w is by assuming that phenotypic changes happen when the energy produced through glucose only is sufficient for cells growth and sustainment their; this allows to define w as independent from oxygen concentration and the rate increases with glucose availability only. This hypothesis is not far from reality: looking back at what has being said about the Warburg effect, even if there are no complete results it is well known that cancer cells are more likely to acquire an anaerobic metabolism even in normoxic conditions.

2.1.5 Boundary conditions and initial conditions

Recalling the equation describing the evolution of $f(t, \mathbf{x}, h)$:

$$\partial_t f + \nabla_{\mathbf{x}} \cdot (f\mathbf{v}) + \partial_h(fw) - \beta\partial_{hh}^2 f = Gf$$

it needs to be supported by boundary conditions in both phenotypic and spatial variables (h and \mathbf{x}).

In order to guarantee that both the transport term $\partial_h(fw)$ and the diffusion term $\beta\partial_{hh}^2f$ do not add any term to the equation of ϕ , obtained integrating with respect to h the function f , Robin's conditions were chosen:

$$f(t, \mathbf{x}, 0)w(0, c_o(t, \mathbf{x}), c_g(t, \mathbf{x})) - \beta\partial_h f(t, \mathbf{x}, 0) = 0 \quad \forall \mathbf{x} \in \bar{\Omega}, \forall t \in (0, T]$$

$$f(t, \mathbf{x}, 1)w(1, c_o(t, \mathbf{x}), c_g(t, \mathbf{x})) - \beta\partial_h f(t, \mathbf{x}, 1) = 0 \quad \forall \mathbf{x} \in \bar{\Omega}, \forall t \in (0, T]$$

Having that $w(0, c_o(t, \mathbf{x}), c_g(t, \mathbf{x})) = w(1, c_o(t, \mathbf{x}), c_g(t, \mathbf{x})) = 0$ for non-catalytic phenotype changes, the boundary conditions becomes:

$$\partial_h f(t, \mathbf{x}, 0) = \partial_h f(t, \mathbf{x}, 1) = 0 \quad \forall \mathbf{x} \in \bar{\Omega}, \forall t \in (0, T]$$

For what concerns the physical space, null flux conditions were imposed:

$$\mathbf{n} \cdot \mathbf{v} = 0 \quad , \quad x \in \partial\Omega$$

Lastly, as initial condition the aim is to mimic a biological scenario in which for $t = 0$ (at the beginning of the process) the phenotype is in state \bar{h}^0 and the highest cell density can be found where the blood vessel is placed, hence in \mathbf{x}_v (coordinates depending on the different domain and blood vessels number and setting). Consequently, a possible initial condition can be:

$$f(0, \mathbf{x}, h) = f_0(\mathbf{x}, h) = C \exp\left(-\frac{\mathbf{x} - \mathbf{x}_v}{\sigma_1} - \frac{(h - \bar{h}^0)^2}{\sigma_2}\right)$$

The condition above describes the exponential decay in space of the number of cells and, for every position \mathbf{x}_v fixed, the cell phenotype is described by a Gaussian centered in \bar{h}^0 .

2.2 Glucose and oxygen dynamic

From now on it is assumed that nutrients, such as oxygen and glucose, are consumed by the cells and that they can enter the domain only through the blood vessel (placed in \mathbf{x}_v , as previously mentioned). The dynamic of nutrients is described by the convection-diffusion equation:

$$\partial_t c_i = D_i \nabla^2 c_i - \sigma_i \zeta_i - \lambda_i c_i, \quad i \in \{o, g\} \quad (15)$$

where:

- D_i is the diffusion coefficient;
- σ_i describes the nutrients consumption due to cancer cells, which depends on how much ATP is produced;
- λ_i is the natural decay of abiotic factors.

The oxygen consumption rate during aerobic respiration for each cell is:

$$Q_o = \frac{6}{36} q_o$$

whereas the glucose consumption rate considering both pathway is:

$$Q_g = \frac{1}{36} q_o + \frac{1}{2} q_g$$

Since the consumption of nutrients is studied from a macroscopic point of view, we have that:

$$\sigma_o = \frac{6}{36} \int q_o n_o(h) f dh \quad (16)$$

$$\sigma_g = \frac{1}{36} \int q_o n_o(h) f dh + \frac{1}{2} \int q_g n_g(h) f dh \quad (17)$$

2.2.1 Boundary conditions and initial conditions

The convection-diffusion equation (15) needs to be supported by boundary and initial conditions. In particular, Dirichlet boundary conditions are used in physical space:

$$c_o(t, \mathbf{x}) = \bar{c}_o(\mathbf{x}) \quad c_g(t, \mathbf{x}) = \bar{c}_g(\mathbf{x}) \quad \text{for } \mathbf{x} \in \partial\Omega \text{ and } t > 0$$

Moreover

$$c_o(0, \mathbf{x}) = c_o^0(\mathbf{x}) \quad c_g(0, \mathbf{x}) = c_g^0(\mathbf{x}) \quad \forall \mathbf{x} \in \Omega$$

Boundary conditions need to be consistent with the position of the nutrient source, hence the position of the blood vessel.

2.3 Qualitative analysis

Considering the model (3) in a bidimensional space $\Omega = [0, L] \times [0, L]$ and assuming that oxygen and glucose concentrations are at equilibrium, so that:

$$c_g(t, \mathbf{x}) = c_g^\infty(\mathbf{x}) \quad c_o(t, \mathbf{x}) = c_o^\infty(\mathbf{x})$$

with $c_g^\infty(\mathbf{x}) : \Omega \rightarrow \mathbb{R}^+$ and $c_o^\infty(\mathbf{x}) : \Omega \rightarrow \mathbb{R}^+$. The dynamic of the function $f = f(t, \mathbf{x}, h)$ is described by:

$$\begin{cases} \partial_t f - \gamma \hat{\mu}(h) \nabla_{\mathbf{x}}[f \nabla_{\mathbf{x}}(\phi)] + \alpha \partial_h(f \hat{w}) = Gf + \beta \partial_{hh}^2 f & \mathbf{x} \in \Omega, h \in (0, 1), \\ \phi = \int_0^1 f(t, \mathbf{x}, h) dh \end{cases} \quad (18)$$

$$\text{with } \gamma \hat{\mu} = \mu \text{ and } \alpha \hat{w} = w \quad (19)$$

with boundary and initial conditions described in the previous section.

The fitness function G is defined as

$$G = G(\mathbf{x}, h, \phi) = \eta(\bar{\phi} - \phi)_+ (\tilde{q}(\mathbf{x}, h) - 1)_+ - \xi - \xi_q(1 - \tilde{q}(\mathbf{x}, h))_+ \quad (20)$$

where \tilde{q} becomes function of \mathbf{x} only through $c_g^\infty(\mathbf{x})$ and $c_o^\infty(\mathbf{x})$.

Rescaled problem.

Cell motion and induced phenotype variation are usually slower than cell proliferation and death. Spontaneous epimutations, instead, are usually slower than induced ones. Because of this, we consider:

$$\alpha := \varepsilon \quad \gamma := \varepsilon \quad \beta := \varepsilon^2$$

where $0 < \varepsilon \ll 1$. In order to consider the dynamic of the system for a time scale corresponding to multiple cell generation, the problem has been rescaled using the time scaling $t \rightarrow \frac{t}{\varepsilon}$. The EDP (18) for $f_\varepsilon(t, \mathbf{x}, h) = f(\frac{t}{\varepsilon}, \mathbf{x}, h)$:

$$\begin{cases} \varepsilon \partial_t f_\varepsilon - \varepsilon \mu(h) \nabla_{\mathbf{x}} f_\varepsilon [\nabla_{\mathbf{x}}(\phi_\varepsilon)] - \varepsilon \mu(h) f_\varepsilon \nabla_{\mathbf{x}}^2(\phi_\varepsilon) + \varepsilon \partial_h(w f_\varepsilon) = G f_\varepsilon + \varepsilon^2 \partial_{hh}^2 f_\varepsilon \\ \phi_\varepsilon = \int_0^1 f_\varepsilon(t, \mathbf{x}, h) dh \end{cases} \quad (21)$$

The target is to analyze the asymptotic behaviour of f_ε for $\varepsilon \rightarrow 0$, which from a biological point of view corresponds to study the phenotypical and spatial dynamic in the limit of multiple cell generations. This analysis takes into account the biologic scenario in which phenotype variations are sporadic with respect to proliferation and death phenomena, as mentioned previously.

Asymptotic analysis for $\varepsilon \rightarrow 0$.

Equation (21) subject to boundary and initial conditions mentioned in previous sections is such that:

$$\text{if } 0 \leq \phi_\varepsilon(0, \mathbf{x}) < \bar{\phi} \quad \forall \mathbf{x} \in \Omega \quad (22)$$

↓

$$0 \leq \phi_\varepsilon(\cdot, \mathbf{x}) < \bar{\phi} \quad \forall \mathbf{x} \in \Omega \quad (23)$$

The bound given by (23) guarantees that $(\bar{\phi} - \phi_\varepsilon)_+ \equiv (\bar{\phi} - \phi_\varepsilon)$, which allows to consider the fitness function as

$$G = G(\mathbf{x}, h, \phi) = \eta(\bar{\phi} - \phi)(\tilde{q}(\mathbf{x}, h) - 1)_+ - \xi - \xi_q(1 - \tilde{q}(\mathbf{x}, h))_+ \quad (24)$$

Now, let us assume that $f_\varepsilon(0, \mathbf{x}, h)$ is a sufficiently regular function that for any fixed value of \mathbf{x} is a Gaussian in h with little variance, corresponding to the biologic scenario in which at the beginning of the dynamic most cells can be found having different spatial positions, but same phenotype. In particular, let us consider a Gaussian function with variance given by parameter ε for every $\mathbf{x} \in \Omega$ and mean described by the function $\bar{h}^0 : \Omega \rightarrow [0, 1]$, whose integral follows condition (22). The function f_ε takes the form:

$$f_\varepsilon(0, \mathbf{x}, h) = \exp \left[\frac{u_\varepsilon^0(\mathbf{x}, h)}{\varepsilon} \right] \quad (25)$$

in which $u_\varepsilon^0(\mathbf{x}, h)$ is a regular function, strictly concave in h and such that:

$$\exp \left[\frac{u_\varepsilon^0(\mathbf{x}, h)}{\varepsilon} \right] \xrightarrow[\varepsilon \rightarrow 0]{*} \phi(0, \mathbf{x})\delta(h - \bar{h}^0(\mathbf{x})) \quad \forall \mathbf{x} \in \Omega \quad (26)$$

Under these assumptions, in the limit $\varepsilon \rightarrow 0$, solutions of (21) are concentrated following a Dirac distribution, as discussed in [12], [13], [7]:

$$f(t, \mathbf{x}, h) \approx \phi(t, \mathbf{x})\delta(h - \bar{h}(\mathbf{x})) \quad (27)$$

From a biological point of view, concentration points of $\bar{h} : \Omega \rightarrow [0, 1]$ represents the phenotype in which the majority of the cancer cell population is found to be at. In this scenario, as it was done by [14] and [15], the WKB ansatz is introduced⁶:

$$f_\varepsilon(t, \mathbf{x}, h) = \exp \left[\frac{u_\varepsilon(t, \mathbf{x}, h)}{\varepsilon} \right] \quad (28)$$

which finds an equation for $u_\varepsilon(t, \mathbf{x}, h)$. Equation (28) can be interpreted as an approximation of Dirac masses $\delta(h - \bar{h}(\mathbf{x}))$ by Gaussian functions ([12], [13]). Computing:

$$\partial_t f_\varepsilon = \frac{f_\varepsilon}{\varepsilon} \partial_t u_\varepsilon, \quad \nabla_{\mathbf{x}} f_\varepsilon = \frac{f_\varepsilon}{\varepsilon} \nabla_{\mathbf{x}} u_\varepsilon, \quad \partial_h f_\varepsilon = \frac{f_\varepsilon}{\varepsilon} \partial_h u_\varepsilon, \quad \partial_{hh}^2 f_\varepsilon = f_\varepsilon \left(\frac{\partial_h u_\varepsilon}{\varepsilon} \right)^2 + \frac{f_\varepsilon}{\varepsilon} \partial_{hh}^2 u_\varepsilon$$

substituting (28) in the EDP (21) we get:

$$\varepsilon \frac{f_\varepsilon}{\varepsilon} \partial_t u_\varepsilon - \varepsilon \mu(h) \frac{f_\varepsilon}{\varepsilon} \nabla_{\mathbf{x}} u_\varepsilon \nabla_{\mathbf{x}} (\phi_\varepsilon \Sigma(\phi_\varepsilon)) - \varepsilon \mu(h) f_\varepsilon \nabla_{\mathbf{x}}^2 (\phi_\varepsilon \Sigma(\phi_\varepsilon)) + \varepsilon w \frac{f_\varepsilon}{\varepsilon} \partial_h u_\varepsilon + \varepsilon f_\varepsilon \partial_h w = \quad (29)$$

$$G f_\varepsilon + \varepsilon^2 \left(\frac{\partial_h u_\varepsilon}{\varepsilon} \right)^2 f_\varepsilon + \varepsilon^2 \frac{f_\varepsilon}{\varepsilon} \partial_{hh}^2 u_\varepsilon \quad (30)$$

which, for u_ε is

$$\partial_t u_\varepsilon - \mu(h) (\nabla_{\mathbf{x}} u_\varepsilon) (\nabla_{\mathbf{x}} (\phi_\varepsilon)) - \varepsilon \mu(h) \nabla_{\mathbf{x}}^2 (\phi_\varepsilon) + w \partial_h u_\varepsilon + \varepsilon \partial_h w = G + (\partial_h u_\varepsilon)^2 + \varepsilon \partial_{hh}^2 u_\varepsilon \quad (31)$$

Taking $\varepsilon \rightarrow 0$ equation (31) becomes:

$$\partial_t u - \mu(h) (\nabla_{\mathbf{x}} u) (\nabla_{\mathbf{x}} (\phi)) + w \partial_h u = G + (\partial_h u)^2, \quad (\mathbf{x}, h) \in \Omega \times (0, 1) \quad (32)$$

⁶Generally, WKB theory is a method for approximating the solution of a differential equation whose highest derivative is multiplied by a small parameter ε . The method of approximation is as follows.

For a differential equation

$$\varepsilon \frac{d^n y}{dx^n} + a(x) \frac{d^{n-1} y}{dx^{n-1}} + \cdots + k(x) \frac{dy}{dx} + m(x)y = 0$$

assume a solution of the form of an asymptotic series expansion

$$y(x) \sim \exp \left[\frac{1}{\delta} \sum_{n=0}^{\infty} \delta^n S_n(x) \right]$$

in the limit $\delta \rightarrow 0$. The asymptotic scaling of δ in terms of ε will be determined by the equation.

Substituting the above ansatz into the differential equation and cancelling out the exponential terms allows one to solve for an arbitrary number of terms $S_n(x)$ in the expansion.

in which u and ϕ are the zero-order terms of the u_ε and ϕ_ε expansions, respectively. A rigorous derivation of (32) is presented in [12], in which the proof relies on several analytical results based on the hypothesis here outlined. Since $u_\varepsilon^0(\mathbf{x}, h) = u_\varepsilon(0, \mathbf{x}, h)$ is a uniformly strictly concave function in h , if the fitness function G is also concave, then it follows that $u(t, \mathbf{x}, h)$ is also uniformly strictly concave in h . Formally we have that for every $\mathbf{x} \in \Omega$ there exist a unique phenotype, described by function $\bar{h}(\mathbf{x}, t)$, such that:

$$u(t, \mathbf{x}, \bar{h}(\mathbf{x})) =: \max_{h \in [0, 1]} u(t, \mathbf{x}, h) \quad \forall \mathbf{x} \in \Omega$$

and

$$\partial_h u(t, \mathbf{x}, \bar{h}(\mathbf{x})) = 0 \quad \forall \mathbf{x} \in \Omega$$

Moreover, based on the bounds described in (23) and the ansatz (28) the following constraint needs to be satisfied:

$$\max_{h \in [0, 1]} u(t, \mathbf{x}, \bar{h}) = u(t, \mathbf{x}, \bar{h}) = 0 \quad , \quad \forall \mathbf{x} \in \text{supp}(\phi) \quad (33)$$

in which the support of $\phi(t, \mathbf{x})$ denotes the set of $\mathbf{x} \in \Omega$ such that $\phi > 0$.⁷ Therefore:

$$\partial_h u(t, \mathbf{x}, \bar{h}(\mathbf{x})) = 0 \quad \nabla_{\mathbf{x}} u(t, \mathbf{x}, \bar{h}) = 0 \quad , \quad \forall x \in \text{supp}(\phi) \quad (35)$$

Lastly, computing equation (32) in $\bar{h}(t, \mathbf{x})$ it can be found that:

$$G(\mathbf{x}, \bar{h}(t, \mathbf{x}), \phi) = 0 \quad , \quad \forall \mathbf{x} \in \text{supp}(\phi(t, \cdot)) \quad (36)$$

Transport equation for $\bar{h}(t, \mathbf{x})$.

Let us now consider $\mathbf{x} \in \text{supp}(\phi(t, \cdot))$. Differentiating equation (32) with respect to h and evaluating the latest in \bar{h} , an equation describing the dynamic of \bar{h} can be found obtaining

$$\partial_{ht}^2 u(t, \mathbf{x}, \bar{h}) - \mu(\bar{h})(\nabla_{\mathbf{x}}(\phi))\partial_h [\nabla_{\mathbf{x}} u(t, \mathbf{x}, \bar{h})] + \partial_h(w\partial_h u)(t, \mathbf{x}, \bar{h}) = \partial_h G \quad (37)$$

Then, differentiating both of the equations found in (35) with respect to t and h respectively, substituting them in (37) and recalling that u is strictly concave in h ($\partial_{hh}^2 u < 0$), the following transport equation for $\bar{h}(t, \mathbf{x})$ can be found

$$\partial_t \bar{h} - \mu(\bar{h})(\nabla_{\mathbf{x}}\phi)(\nabla_{\mathbf{x}}\bar{h}) = (-\partial_{hh}^2 u(t, \mathbf{x}, \bar{h}))^{-1}(\partial_h G(\mathbf{x}, \bar{h}, \phi) - \partial_h(w\partial_h u)(t, \mathbf{x}, \bar{h})) \quad (38)$$

with $\mathbf{x} \in \text{supp}(\phi)$.

Limits of $\phi(t, \mathbf{x})$ and $\bar{h}(t, \mathbf{x})$ for $t \rightarrow \infty$.

Defining $\phi^\infty(\mathbf{x})$ and $h^\infty(\mathbf{x})$ the asymptotic values to which $\phi(t, \mathbf{x})$ and $\bar{h}(t, \mathbf{x})$ converge for $t \rightarrow \infty$. Taking into account (36) and the transport equation described in (38) that corresponds to the steady state equation, $\phi^\infty(\mathbf{x})$ and $\bar{h}^\infty(\mathbf{x})$ need to satisfy the following:

$$\begin{cases} G(\mathbf{x}, \bar{h}^\infty, \phi^\infty) = 0 & (\text{defines } \phi^\infty) \\ [-\mu(h)(\nabla_{\mathbf{x}}\phi^\infty)\nabla_{\mathbf{x}}h]_{h=\bar{h}^\infty} = \mathcal{F}(\mathbf{x}, \bar{h}^\infty, u^\infty, \phi^\infty) & (\text{defines } \bar{h}^\infty) \end{cases} , \quad \mathbf{x} \in \text{supp}(\phi^\infty) \quad (39)$$

in which

$$\mathcal{F}(\mathbf{x}, h^\infty, u^\infty, \phi^\infty) := -(\partial_{hh}^2 u(\mathbf{x}, h))^{-1}(\partial_h G(\mathbf{x}, h, \phi^\infty) - \partial_h(w\partial_h u^\infty)(\mathbf{x}, h))$$

⁷This discussion is inserted in a more general mathematical framework concerning *constrained Hamilton-Jacobi equations*. Their analysis is beyond the scope of this paper, but the following remark can be highlighted. As discussed in [13], from a PDE point of view, in the system:

$$\begin{cases} \partial_t u - \mu(h)(\nabla_{\mathbf{x}} u)(\nabla_{\mathbf{x}}(\phi)) + w\partial_h u = G + (\partial_h u)^2 & , \quad (\mathbf{x}, h) \in \Omega \times (0, 1), \\ \max_{h \in [0, 1]} u(t, \mathbf{x}, \bar{h}) = u(t, \mathbf{x}, \bar{h}) = 0 & , \quad \forall \mathbf{x} \in \text{supp}(\phi) \end{cases} \quad (34)$$

$\phi(t, \mathbf{x})$ is a Lagrange multiplier associated with the constraint (33). More information about Hamilton-Jacobi equations and their application in adaptive dynamics can be found in literature, e.g. [12], [13].

and where u^∞ satisfy the steady state transport equation (32) subject to (33) which is

$$\begin{cases} G(\mathbf{x}, h, \phi^\infty) + (\partial_h u^\infty(\mathbf{x}, h))^2 - w \partial_h u^\infty(h) = 0 & \mathbf{x} \in \text{supp}(\phi^\infty) \\ \max_{h \in [0,1]} u^\infty(\mathbf{x}, h) = u^\infty(\mathbf{x}, \bar{h}^\infty(\mathbf{x})) = 0 \end{cases} \quad (40)$$

The first equation of system (39) is analyzed after substituting the definition of the fitness function written in (24):

$$G(\mathbf{x}, \bar{h}^\infty, \phi^\infty) = 0 \implies \eta(\bar{\phi} - \phi^\infty(\mathbf{x}))(\tilde{q}(\mathbf{x}, \bar{h}^\infty(\mathbf{x})) - 1)_+ - \xi - \xi_q(1 - \tilde{q}(\mathbf{x}, \bar{h}^\infty(\mathbf{x})))_+ = 0 \quad (41)$$

for $\mathbf{x} \in \text{supp}(\phi^\infty)$.

For what concerns the positive part there are three possible scenarios, one excluding the other:

- $\tilde{q}(\mathbf{x}, \bar{h}^\infty) = 1 \implies (1 - \tilde{q}(\mathbf{x}, \bar{h}^\infty(\mathbf{x})))_+ = (\tilde{q}(\mathbf{x}, \bar{h}^\infty(\mathbf{x})) - 1)_+ = 0$
- $(\tilde{q}(\mathbf{x}, \bar{h}^\infty(\mathbf{x})) - 1)_+ = 0 \implies (1 - \tilde{q}(\mathbf{x}, \bar{h}^\infty(\mathbf{x})))_+ > 0$
- $(\tilde{q}(\mathbf{x}, \bar{h}^\infty(\mathbf{x})) - 1)_+ > 0 \implies (1 - \tilde{q}(\mathbf{x}, \bar{h}^\infty(\mathbf{x})))_+ = 0$

Analysing these three scenarios and substituting each one of them in (41), the first and second cases result as absurd statements, whereas the third one results in an equation for $\phi^\infty(\mathbf{x})$

$$\tilde{q}(\mathbf{x}, \bar{h}^\infty(\mathbf{x})) > 1 , \quad \mathbf{x} \in \text{supp}(\phi^\infty) \quad (42)$$

$$\Downarrow \\ 0 = \eta(\bar{\phi} - \phi^\infty(\mathbf{x}))(\tilde{q}(\mathbf{x}, \bar{h}^\infty(\mathbf{x})) - 1)_+ - \xi \quad (43)$$

Since $\phi^\infty(\mathbf{x}) \geq 0 \quad \forall \mathbf{x} \in \Omega$, as stated in (23), if

$$\bar{\phi} - \frac{\xi}{\eta} \frac{1}{(\tilde{q}(\mathbf{x}, \bar{h}^\infty(\mathbf{x})) - 1)} < 0$$

then (43) does not allow non-negative solutions $\phi^\infty(\mathbf{x})$ and consequently $\mathbf{x} \notin \text{supp}(\phi^\infty)$, that is $\phi^\infty(\mathbf{x}) = 0$. Otherwise

$$\phi^\infty(\mathbf{x}) = \bar{\phi} - \frac{\xi}{\eta} \frac{1}{(\tilde{q}(\mathbf{x}, \bar{h}^\infty(\mathbf{x})) - 1)} \quad (44)$$

Concluding, it has been found that

$$\phi^\infty(\mathbf{x}) = \max \left\{ 0, \bar{\phi} - \frac{\xi}{\eta} \frac{1}{(\tilde{q}(\mathbf{x}, \bar{h}^\infty(\mathbf{x})) - 1)} \right\} \quad (45)$$

2.4 Case study: only spontaneous phenotype changes

The only case that will be studied and tested in this work considers equation (39) for the scenario in which there is no motion in physical space and there are no induced phenotype changes. This scenario can also be summarized saying that $\mathbf{v} \equiv 0$ and $w \equiv 0$. From the second equation of (39) it follows that:

$$[\partial_h G(h, \phi^\infty)]_{h=\bar{h}^\infty} = 0 \quad (46)$$

obtaining $\eta(\bar{\phi} - \phi^\infty)\partial_h(\tilde{q} - 1)_+(\bar{h}^\infty) - \xi_q\partial_h(1 - \tilde{q})_+(\bar{h}^\infty) = 0$.

Recalling (42), the previous equation can be simplified as:

$$\eta(\bar{\phi} - \phi^\infty)\partial_h\tilde{q}(\bar{h}^\infty) = 0$$

Since $\eta > 0$ and $\bar{\phi} - \phi^\infty > 0$ it needs to be:

$$\bar{h}^\infty = \arg \max_{h \in [0,1]} \tilde{q} \quad (47)$$

Which means that phenotype \bar{h}^∞ is the one that maximizes not only the proliferation function \tilde{q} , but also the volume fraction occupied by cancer cells ϕ^∞ .

2.4.1 Fitness function G

- **Linear** (with respect to h) proliferation function q :

$$q = (1 - h)q_o + hq_g$$

Meaning that the fitness function $G(x, h, \phi)$ is a monotone function with respect to h in $[0, 1]$ which allows a unique maximum point. Therefore, it can also be assumed that function u is strictly convex in h in order to study the system in (39).

The first equation of the system results, again, in equation (45), but the derivative with respect to h of the fitness function G results in

$$\bar{h}^\infty = \operatorname{argmax}_{h \in [0, 1]} \tilde{q}$$

but

$$\partial_h \tilde{q} = \frac{q_g - q_o}{\theta} \quad (48)$$

Which means that

$$\bar{h}^\infty = \begin{cases} 1, & \text{if } q_g > q_o \\ 0, & \text{if } q_g < q_o \end{cases} \quad (49)$$

Instead, if $q_g = q_o$, then $\tilde{q} = \frac{q_o}{\theta}$ is a constant function, which *does not* depend on h and therefore whatever value of h satisfies the second equation of (39). From a biological point of view the scenario that has just been discussed is not particularly relevant since the model is such that we either have $(\tilde{q} - 1)_+ > 0$ or $(1 - \tilde{q})_+ > 0$ or $\tilde{q} = 1$.

- **Quadratic** (with respect to h) proliferation function:

$$q = (1 - h^2)q_o + h^2q_g$$

The maximum value of the function is given by the sign of $q_g - q_o$.

Instead, if the quadratic function is of the form

$$q = (1 - h^2)q_o + [1 - (1 - h)^2]q_g \quad (50)$$

describing a parabolic function with downward concavity and an unique maximum point:

$$\partial_h q = 2[-hq_o + (1 - h)q_g] = 0 \iff h = \frac{q_g}{q_o + q_g} \quad (51)$$

This scenario is assuming that the fitness function G , for every point in space, has a unique maximum point in h which is, biologically speaking, more relevant than the linear one and, for this reason, adopted in the current study.

3 Numerical Simulations

The study takes into account two different domain cases:

- **mono-dimensional** in space, i.e. $\Omega = [0, L]$, and in phenotype $h \in [0, 1]$;
- **bi-dimensional** case in space, i.e. $\Omega \in [0, L] \times [0, L]$ and mono-dimensional in phenotype $h \in [0, 1]$.

The following numerical simulations have been carried out using Comsol Multiphysics[®], whose methods are based on FEM discretization.

In order to discretize the model equations, it has been necessary creating an appropriate mesh of the domain: in the cases that has been studied a regular triangular mesh was sufficient in order to obtain good results and reach convergence after little amount of time. Specifically, the number of degrees of freedom for the mono-dimensional case was 5209 (plus 284 internal ones) and for the bi-dimensional case was 7311 (plus 1774 internal ones).

Since the model includes a partial integro-differential equation, a time discretization was also needed; taking advantage of Comsol's native tools, an adaptive time step algorithm was selected in order to observe the BDF's⁸ stability.

Then, to deal with the integral $\phi(t, x) = \int_0^1 f(t, x, h)dh$ a specific Comsol's tool was used: the operators of nonlocal *Linear Projection*, for what concerns the mono-dimensional case, and the *General Projection*⁹, for the bi-dimensional case.

In order to converge to a numerical solution and to reach stability, it has been necessary including an *artificial diffusion* term in the space variable. Even with this correction, results obtained simulate a realistic biologic scenario in which the artificial diffusion can be thought as a term describing the casual motion of cells in space.

All the parameters used in the numerical simulations, for both domain and different scaling and settings, are displayed in the Table 3.3 at the end of the section.

3.1 Mono-dimensional scenario

The numerical simulations were carried out using fixed oxygen and glucose concentrations in order to compare the results with the ones from the formal asymptotic analysis. According to this framework, it is assumed $t \in [0, T]$, with the final time T such that the numerical solutions are sufficiently close to equilibrium at the end of the simulations.

In section 2.3 it has been said that function G needs to have a single maximum point in $h \in [0, 1]$, which means that it exist only one state that maximizes the fitness function. In order to meet this request, functions (9) are defined as:

$$n_o(h) = 1 - h^2 \quad n_g(h) = 1 - (1 - h^2) \quad (52)$$

Boundary conditions analysed in section 2.2.1 corresponding to the edge $\mathbf{x} = \mathbf{0}$ have been chosen as:

$$c_o(t, \mathbf{0}) = \bar{c}_o = 2.08 \times 10^{-6} \text{ g cm}^{-3} \quad c_g(t, \mathbf{0}) = \bar{c}_g = 1.35 \times 10^{-4} \text{ g cm}^{-3}$$

These values are the average level of oxygen and glucose near the blood vessel ($x_v = 0$), in agreement with [17]. According to [17], far away from the blood vessel (i.e. at distance L), oxygen and glucose concentrations have values that reach respectively the 0.1% and 1% of \bar{c}_o and \bar{c}_g so that:

$$c_o(t, L, L) = \underline{c}_o = 2 \times 10^{-10} \text{ g cm}^{-3} \quad c_g(t, L, L) = \underline{c}_g = 1.35 \times 10^{-6} \text{ g cm}^{-3}$$

as also suggested in [3]. The simulation has been carried out considering such concentration values, which have then been normalized with respect to the concentration in the boundary $x = 0$.

Assuming that abiotic factors are concentrated in correspondence to the blood vessel (placed at $x_v = 0$), decaying in space as exponentials (figure 3a and 3b), we have:

$$\tilde{c}_o = \exp\left(\frac{x}{L} \ln(\underline{c}_o)\right) \quad \tilde{c}_g = \exp\left(\frac{x}{L} \ln(\underline{c}_g)\right)$$

in which

$$\underline{c}_o = \frac{c_o}{\bar{c}_o} \quad \underline{c}_g = \frac{c_g}{\bar{c}_g}$$

The functions that describes the availability of oxygen and glucose (figure 3c and 3d) are introduced and discussed in section 2.1.1 as:

$$a(c_o) = \frac{c_o}{M_o + c_o} \quad b(c_g) = \frac{c_g}{M_g + c_g}$$

⁸The backward differentiation formula (BDF) is a family of implicit methods for the numerical integration of ordinary differential equations. They are linear multistep methods that, for a given function and time, approximate the derivative of that function using information from already computed time points, thereby increasing the accuracy of the approximation.

⁹More information and technicalities for both the Linear and General Projection operators can be found in [16].

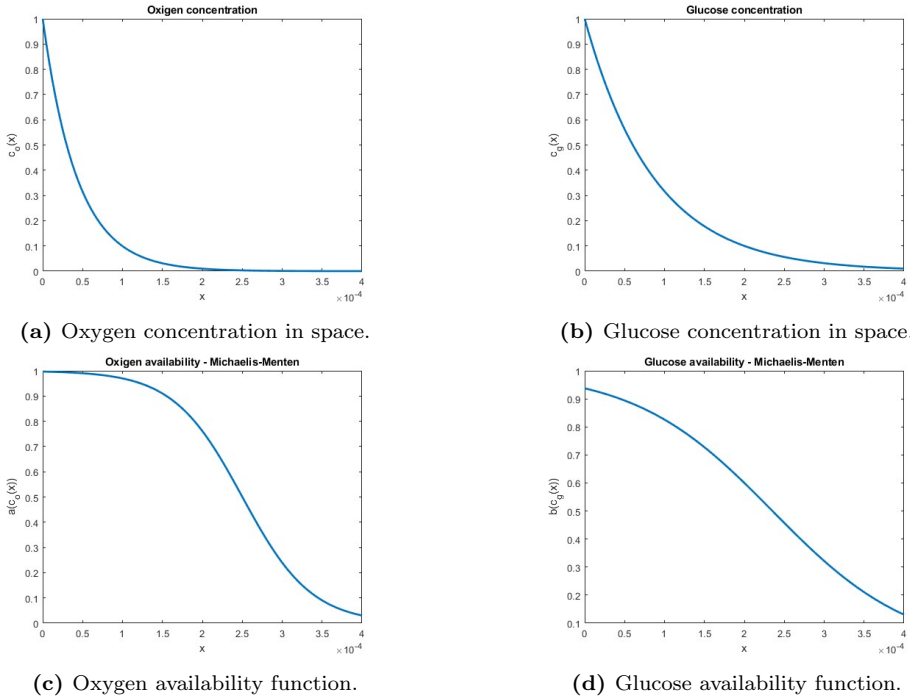


Figure 3

In addition, the proliferation function that has been chosen for the simulations is the one described in (50). Some of the unknown variables such as κ_0 and θ has been arbitrarily chosen, according to the biological problem and the results found thanks to the qualitative analysis.

The initial condition for function f is given by

$$f(0, x, h) = f_0(x, h) := 0.5 \exp\left(-\frac{x}{\sigma_1} - \frac{(h - 0.5)^2}{\sigma_2}\right)$$

describing the scenario in which the number of cells exponentially decreases in space and for every fixed position in space, x , the phenotype is distributed as a Gaussian with 0.5 mean and σ_2 variance.

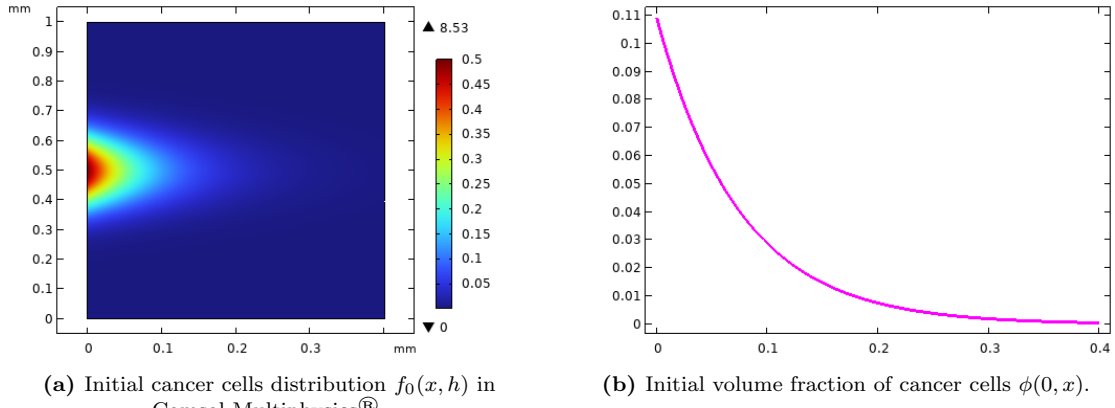


Figure 4

Notice that the initial condition satisfies $0 < \phi(0, x) < 1$, as it is shown in figure 4b.

3.2 Bi-dimensional scenario

These numerical simulations were also carried out using fixed oxygen and glucose concentrations, supposing that they are found at their equilibrium.

The considerations made in the previous section for function G , $a(c_o)$ and $b(c_g)$ in the mono-dimensional scenario can be also made for the bi-dimensional one.

Different settings were then taken into account, in particular:

- the presence of **one vessel only**, placed at the origin of the plane $(x_v, y_v) = (0, 0)$ (low left vertex of Ω). Assuming, again, that the abiotic factors are concentrated in correspondence of the blood vessel, decaying in space as exponentials (5a and 5b), we have:

$$\tilde{c}_o(x, y) = \exp\left(\frac{x+y}{L} \ln(\underline{c}_o)\right) \quad \tilde{c}_g(x, y) = \exp\left(\frac{x^2+y^2}{L^2} \ln(\underline{c}_g)\right)$$

in which \underline{c}_o and \underline{c}_g are defined as in the previous section.

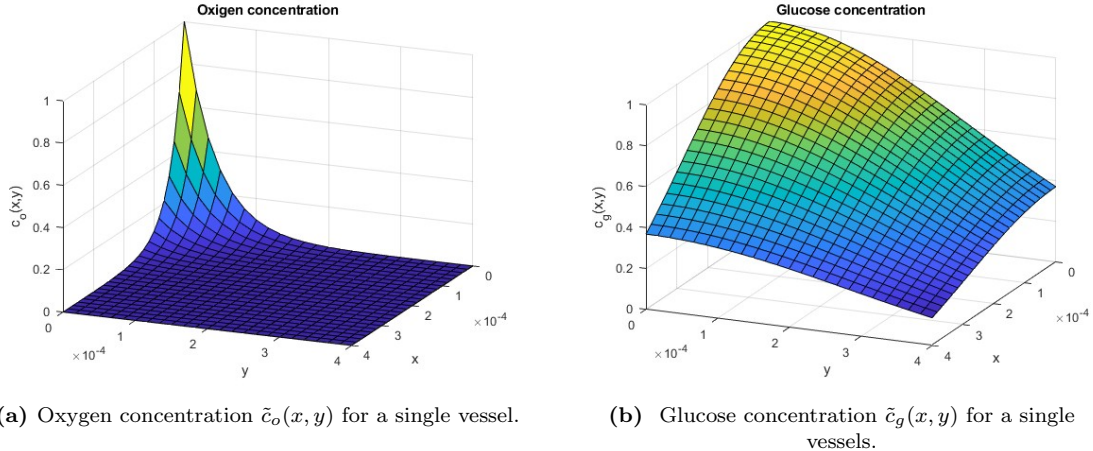


Figure 5

Two different initial conditions were taken into account: the first one following the one used in the mono-dimensional case (decaying in space as exponentials and Gaussian in phenotype), whereas the second one is a spatial uniform condition (and still exponentially decaying in phenotype), as done by [7]. The initial conditions are, respectively:

$$f(0, x, y, h) = f_0(x, y, h) := 0.5 \exp\left(-\frac{x+y}{\sigma_1} - \frac{(h-0.5)^2}{\sigma_2}\right) \quad (53a)$$

$$f(0, x, y, h) = f_0(x, y, h) = f_0(h) := 0.5 \exp\left(\frac{(h-0.5)^2}{\sigma_h}\right) \quad (53b)$$

- the presence of **multiple vessels**, placed inside the domain Ω . Assuming, again, that the abiotic factors are concentrated in correspondence of the blood vessel, *decaying in space as a multivariate Gaussian* (7a and 7b), we have:

$$\begin{aligned} \tilde{c}_o(x, y) &= \sum_{n=0}^m \exp\left(\frac{(x-x_n)^2 + (y-y_n)^2}{L^2 \sigma_{c_o}} \ln(\underline{c}_o)\right) \\ \tilde{c}_g(x, y) &= \sum_{n=0}^m \exp\left(\frac{(x-x_n)^2 + (y-y_n)^2}{L^2 \sigma_{c_g}} \ln(\underline{c}_g)\right) \end{aligned}$$

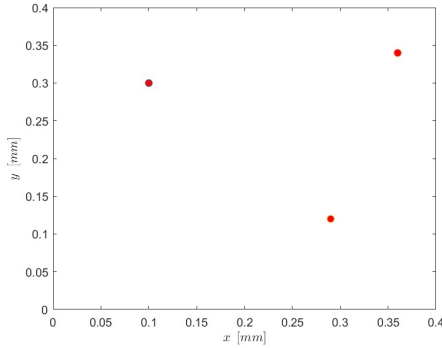
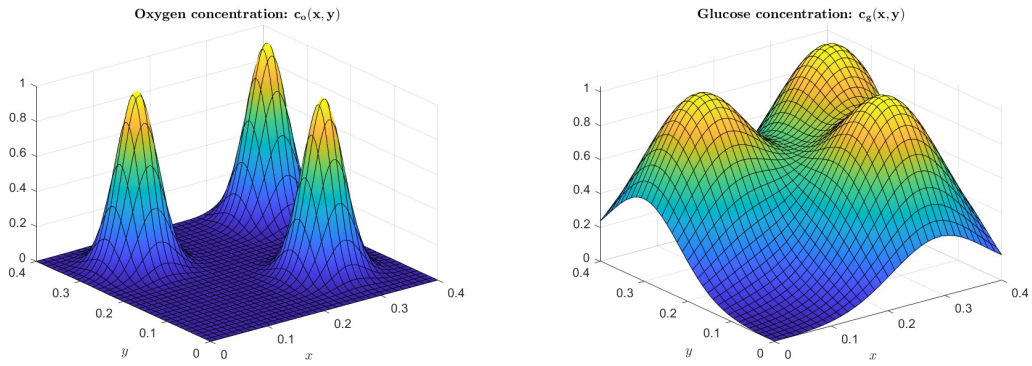


Figure 6: Configuration of the three vessels in Ω .



(a) Oxygen concentrations $\tilde{c}_o(x, y)$ for three vessels as in figure 6.
(b) Glucose concentrations $\tilde{c}_g(x, y)$ for three vessels as in figure 6.

Figure 7

For what concerns this study, the less demanding scenario with three vessels ($m = 3$) inside the domain was considered (figure 6), but a much higher number of vessels could have been considered too.

For multiple vessels the only initial condition considered was the uniform one, as the results are comparable with the one found in [7]:

$$f_0(x, y, h) = f_0(h) := 0.5 \exp\left(\frac{(h - 0.5)^2}{\sigma_h}\right)$$

3.3 Case study: spontaneous phenotype changes only

In this particular scenario $\mathbf{v} \equiv 0$ and $w \equiv 0$ in the evolutionary equation (3) for f , which results in solving the following diffusion-reaction equation in the phenotype variable:

$$\partial_t f - \beta \partial_{hh}^2 f = Gf$$

From equations (51), (45) in section 2.4:

$$\bar{h}^\infty = \frac{q_g}{q_o + q_g}, \quad \phi^\infty(x) = \max \left\{ 0, \bar{\phi} - \frac{\xi}{\eta} \frac{1}{(\tilde{q}(x, \bar{h}^\infty(\mathbf{x})) - 1)} \right\}, \quad x \in [0, L] \quad (55)$$

Now, recalling the definitions of q_o and q_g in (7) we have that

$$\bar{h}^\infty = \frac{q_g}{q_o + q_g} = \frac{2\kappa_g b(c_g)}{36\kappa_o a(c_o)b(c_g) + 2\kappa_g b(c_g)} = \frac{1}{\frac{9}{5}a(c_o) + 1} \quad (56)$$

which means that, at the end, \bar{h}^∞ only depends on the function $a(c_o)$, which in this scenario is of Michealis-Menten type.

Parameter	Value	Reference
M_o	$6.4 \times 10^{-9} \text{ g cm}^{-3}$	[17]
M_g	$9 \times 10^{-6} \text{ g cm}^{-3}$	[17]
β	$3 \times 10^{-19} \text{ s}^{-1}$	ad hoc
γ	10^{-12} s^{-1}	ad hoc
α	$10^{-18} \text{ m}^3 \text{ s kg}^{-1}$	ad hoc
η	$3.54 \times 10^{-7} \text{ s}^{-1}$	-
O_m	$8.2 \times 10^{-9} \text{ g cm}^{-3}$	[18]
O_M	$4.3 \times 10^{-7} \text{ g cm}^{-3}$	[18]
ξ	$2.5 \times 10^{-7} \text{ s}^{-1}$	[19]
ξ_g	ξ	-
E	100 Pa	ad hoc
κ_o	$\frac{1}{3} \text{ s}^{-1}$	ad hoc
κ_g	$10 \times \kappa_o$	ad hoc
L	$4 \times 10^{-4} \text{ m}$	[3]
$\bar{\mu}$	0.001	[15]
ϕ	1	-
θ	0.85	-
σ_1	0.1	-
σ_2	0.015	-
σ_{c_o}	0.1	-
σ_{c_g}	0.4	-
σ_h	σ_2	-

4 Results

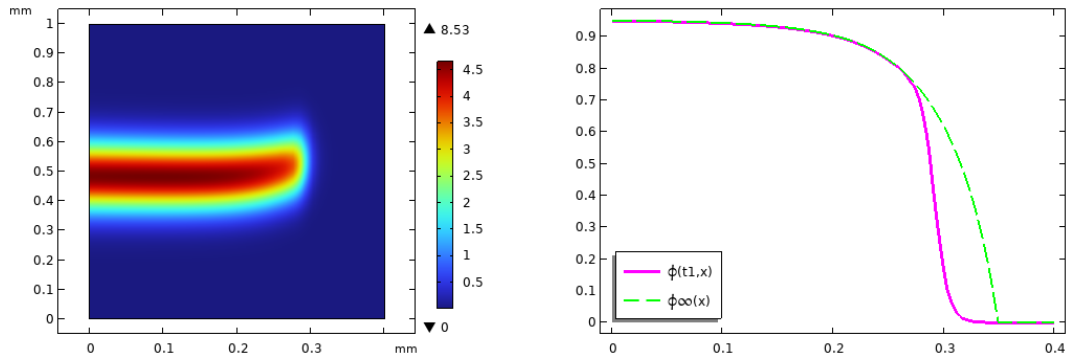
4.1 Mono-dimensional case

In this section the analytical values of $\phi^\infty(x)$ are compared with the volume fraction $\phi(T, x)$ in which T is the last instant of time that has been simulated. Results are found to be consistent with the formal qualitative analysis, as shown in the figures below (11a and 11b). Even if the last instant of time simulated, corresponding to $T = 6000$ days, represents an unlikely biological scenario, it was still chosen in order to verify the asymptotic analysis.

In figure (8), (9), (10) the evolution of the function $f(t, x, h)$ (left panel) and the analytical result of $\phi(t, x)$ (right panel) is provided at different times. The solution $f(t, x, h)$, initially concentrated in $x = 0$ and $h = 0.5$, at a time $t_1 = 150$ days, due to oxygen and glucose availability, shows that cancer cells starts to proliferate, swarming a large part of the expected volume fraction, but with a very small variation on their phenotype.

Looking at a longer time, such as $t_2 = 1000$ days (shown in figure 9b), almost the whole expected volume fraction has been occupied and, in addition, cells started to change their phenotype moving from the initial conditions to a situation in which h is getting greater than the initial value $h = 0.5$. This behaviour gets more and more evident as time goes on, as shown in figure 10a and 11a: the phenotype gets greater and greater than $h = 0.5$ when cells are further and further from the vessel, located in $x_v = 0$.

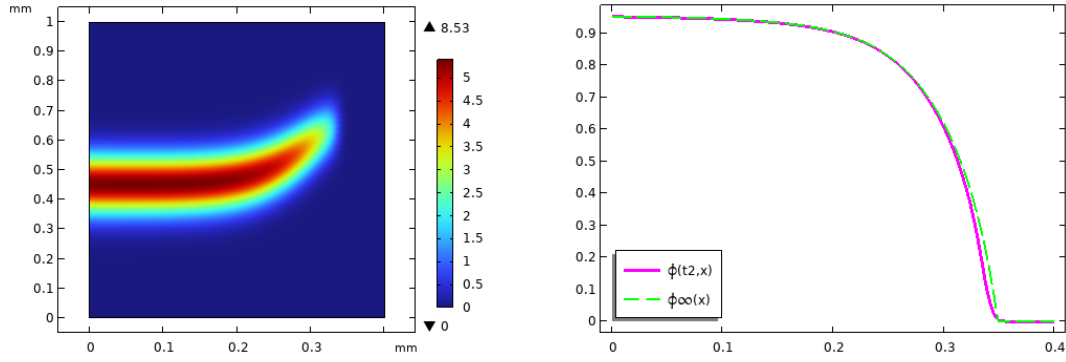
From the biological point of view, the rising in phenotype values further from the vessel implies the selection of cells with an anaerobic metabolism, whereas closer to the vessel, where most of the oxygen is available, the phenotype lowers with respect to the initial value that implies the selection of cells with an aerobic metabolism.



(a) Cancer cells distribution $f(150, x, h)$.

(b) Comparison between the asymptotic volume fraction of cancer cells $\phi^\infty(x)$ and the numerical one $\phi(150, x)$.

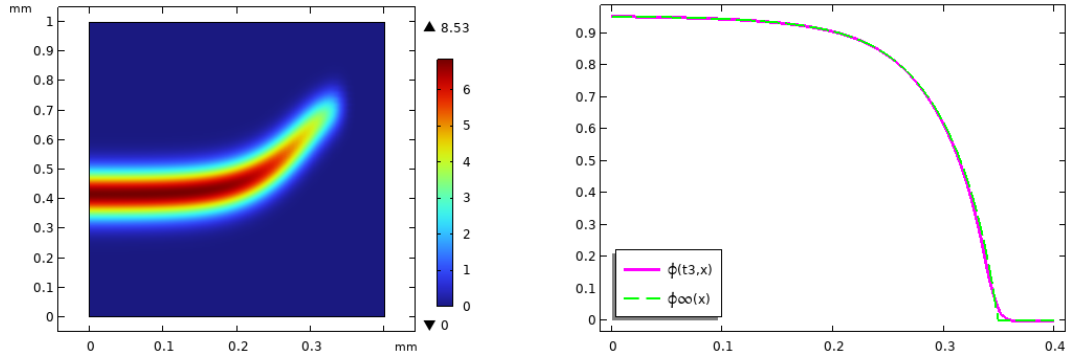
Figure 8



(a) Cancer cells distribution $f(1000, x, h)$.

(b) Comparison between the asymptotic volume fraction of cancer cells $\phi^\infty(x)$ and the numerical one $\phi(1000, x)$.

Figure 9



(a) Cancer cells distribution $f(3000, x, h)$.

(b) Comparison between the asymptotic volume fraction of cancer cells $\phi^\infty(x)$ and the numerical one $\phi(3000, x)$.

Figure 10

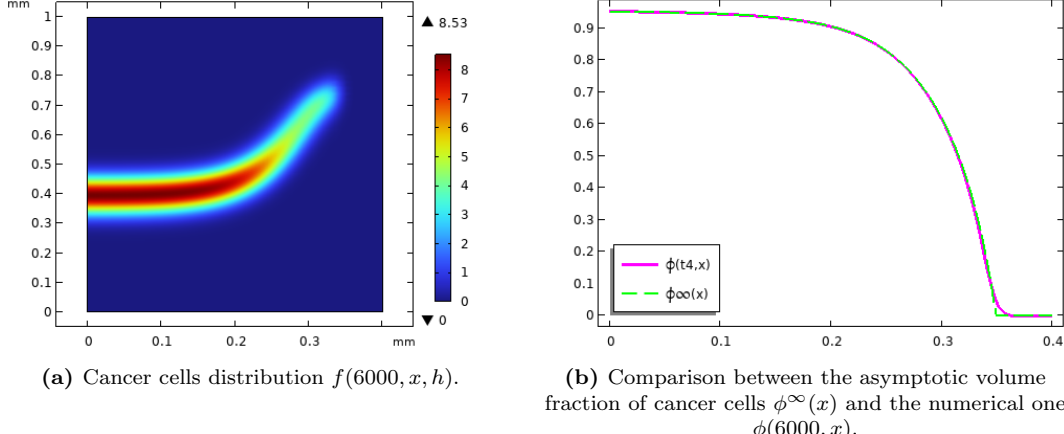


Figure 11

4.2 Bi-dimensional case

In this section a generalization of the mono-dimensional scenario to a bi-dimensional spatial domain is presented, giving a more realistic view of the problem. Different initial conditions and functions for the nutrients availability were used as mentioned in section 3.2.

In particular, biological evidence shows that glucose is often present inside tissues, so that it is not a discerning element in the metabolic switch, element that is instead represented by the oxygen. This is the reason why the functions $c_o(x, y)$ and $c_g(x, y)$ were chosen with high gradients in a neighbourhood of the vessel and almost uniform in the whole domain, respectively.

Following the previous analysis (section 4.1), the study firstly aims at generalizing the main functions of the mono-dimensional scenario and comparing the results given by the two domains. Later, new initial conditions, nutrients concentration functions and vessels settings were adopted and the results compared with the ones found by [7].

Before starting with the results analysis, three remarks should be made:

1. For what concerns this scenario, the last instant of time simulated was chosen to be $T = 700$ days, both because it is not of interest to provide and verify another asymptotic analysis and because it is very computationally demanding. In this section, in fact, the objective is to focus the study on the phenomenological and biological aspects of the dynamic.
2. Still following [20] and differently from what has been done by [7], nutrients concentration functions ($c_o(x, y)$ and $c_g(x, y)$) were assumed to be in their steady states, i.e. without any time dependency.
3. Below numerical results are shown with a recurrent pattern: the volume showing the cancer cells distribution $f(t, x, y, h)$ on the domain (physical domain corresponding to the horizontal and longitudinal direction and phenotypical domain corresponding to the vertical one), the volume fraction of cancer cells $\phi(t, x, y)$ (equation (1)) and the average phenotype distribution $H(t, x, y)$ (equation (2)).

4.2.1 One vessel - Gaussian and uniform initial condition

Results show that an initial condition (Figure 12a), describing an exponential decay in space and a Gaussian distribution in phenotype as in equation (53a), follows a dynamic that generalises results shown in the mono-dimensional case. In fact, the rising in phenotype values far away from the vessel and the lowering of them close to it can still be seen in figures 12b and 12c.

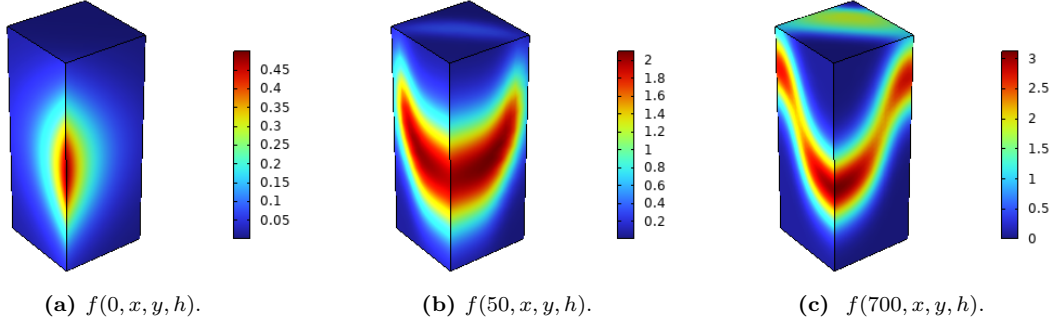


Figure 12: Cancer cells distribution.

Simulations shown in figure (13) display an increase in the volume fraction of cancer cells as time goes on. In particular, at time $t = 0$ (Figure 13a) the fraction is concentrated around the vessel, but as time passes ($t_1 = 50$, figure 13b, and $t_2 = 700$ days, figure 13c) cancer cells invade the domain more and more, though keeping the same maximal and minimal values. It can be also noted that, as it happened for the mono-dimensional scenario, even though anaerobic cancer cells outnumber aerobic ones, they still do not occupy the domain entirely.

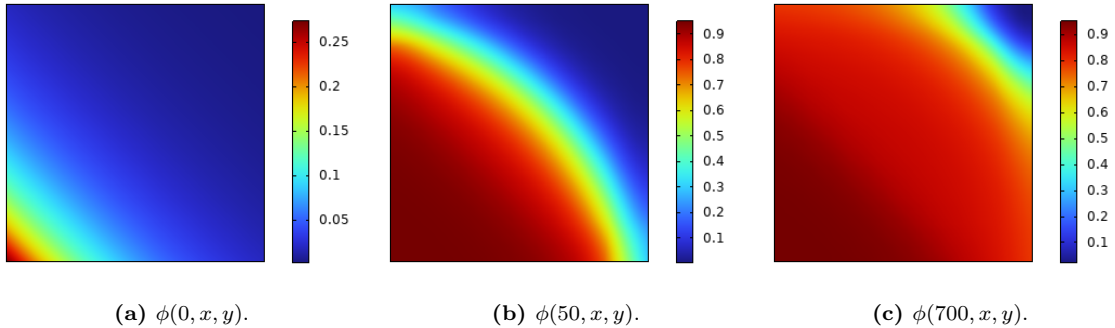


Figure 13: Volume fraction of cancer cells.

A significant change can be found in the average phenotype distribution $H(x, y, t)$, which starting from a uniform distribution (Figure 14a), almost immediately changes its configuration with an evident differentiation between the two kinds of metabolism. As time goes on the distribution changes, leading to a situation in which the anaerobic metabolism, further and further from the vessel, is preferred (Figures 14b, 14c).

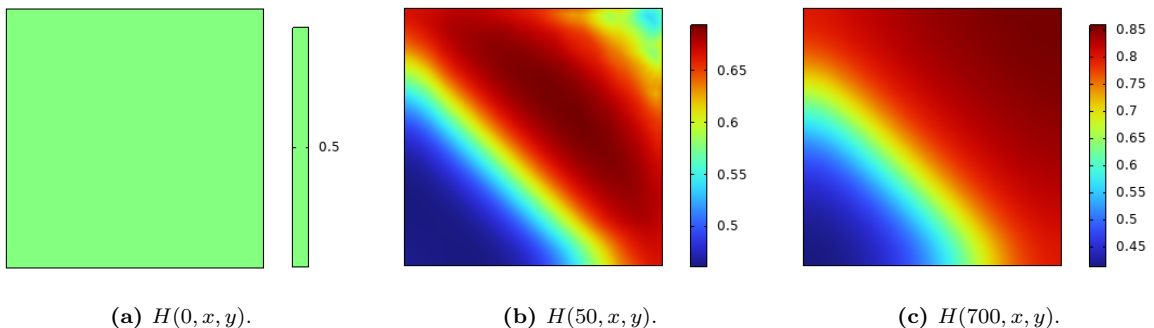


Figure 14: Average phenotype distribution.

Changing instead the initial condition to a space independent and Gaussian in phenotype distribution (Figure 15a), it can be found that even if at time $t = 0$ the configurations are, in general, different from the previous case, the last simulated instant of time ($T = 700$ days) shows comparable, or even superimposable, results. This being said, the same considerations as the ones from the previous scenario, for all the variables taken into account can be made for longer times (Figures 15b, 16b, 16d).

It can also be noticed that at the start of the simulations both the volume fraction and the average phenotype distribution are uniform (Figures 16a, 16c). This remark highlights how the results are likely independent from initial conditions, since they follow from oxygen and glucose concentrations and their interplay with cancer cells (e.g. nutrients consumption and metabolic switch).

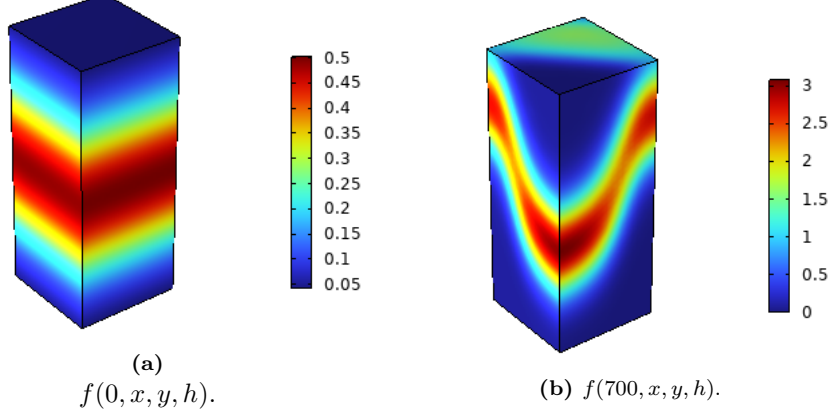


Figure 15: Cancer cells distribution.

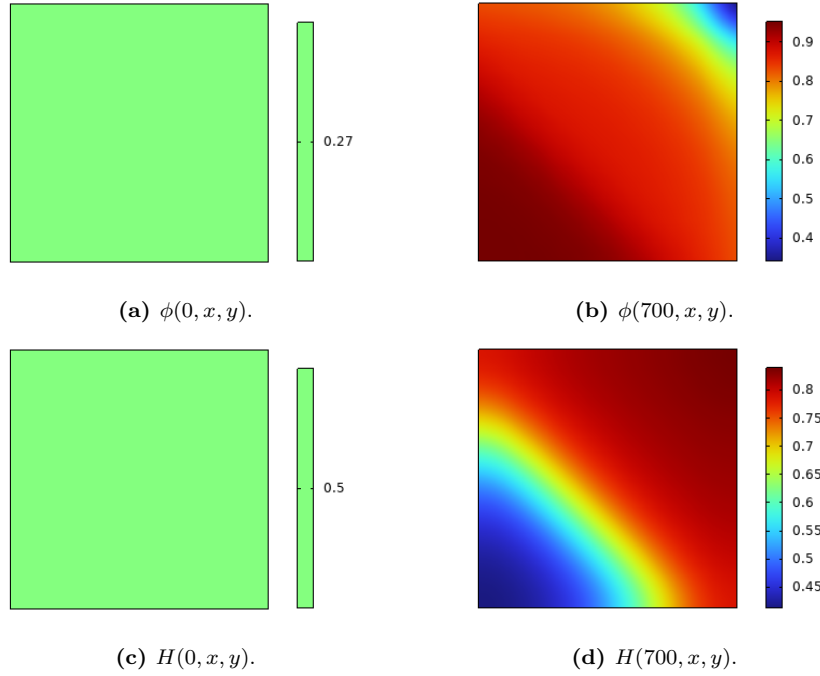
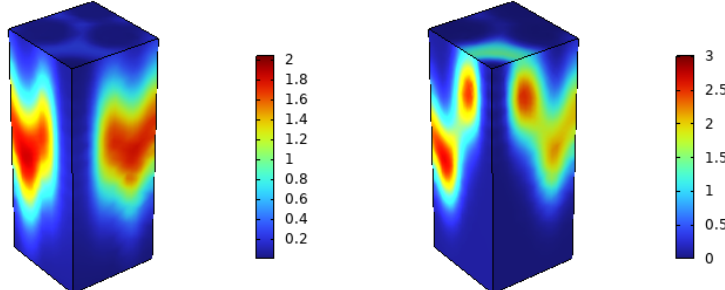


Figure 16: Volume fraction of cancer cells (16a, 16b) and average phenotype distribution (16c, 16d).

4.2.2 Three vessels - uniform initial condition

Since initial conditions do not have a significant relevance on the evolution of the dynamic, without loss of generality they were set as in equation (53b), so the results for time $t = 0$ days and three vessels are exactly the same as the ones in figures (15a), (16a), (16c).

Starting from a situation in which the distribution of cells is uniform in space and mostly concentrated around the phenotype value $h = 0.5$, as time goes on cancer cells grow in number and migrate in space towards the vessels. As expected, a migration in the phenotypical space also occurs, i.e. cancer cells proximal to the vessels lower their phenotype, whereas the ones further from them switch their metabolism into an anaerobic one. This phenomena leads to the emergence of the intratumoral phenotypical heterogeneity as a response to the non-uniform nutrients spatial concentrations (cfr figure (18)).



(a) $f(50, x, y, h)$.

(b) $f(700, x, y, h)$.

Figure 17: Cancer cells distribution.

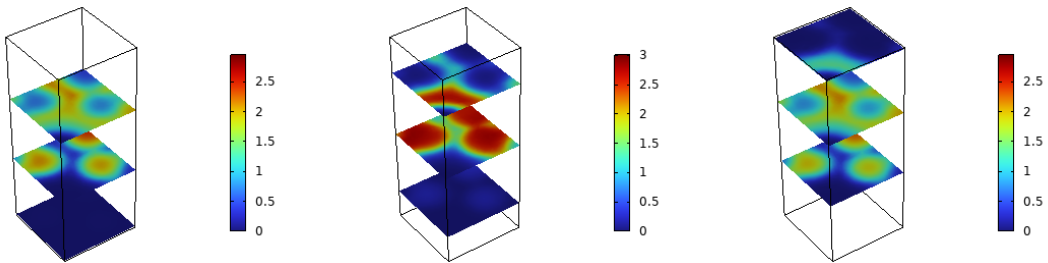
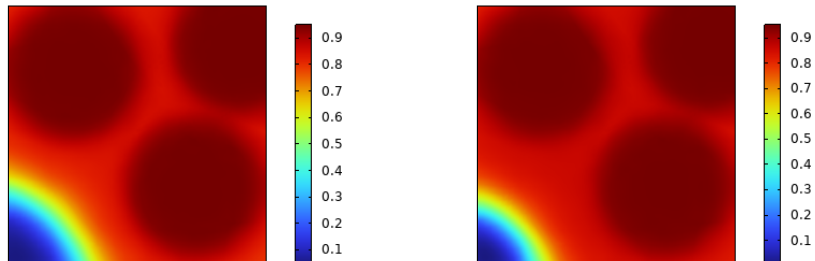


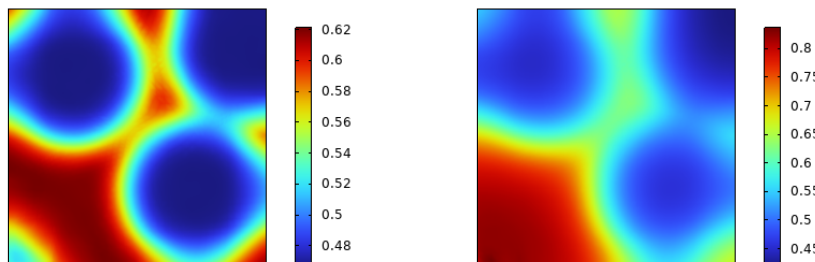
Figure 18: Slicing of f (cancer cells distribution) at time $T = 700$ days.

All considerations done so far can be better seen when looking at the volume fraction of cancer cells and the average phenotype distribution: the higher number of cells can be found near and around the three vessels considered (cfr. 19a, 19b), but their phenotype is lower than the ones far from the vessels. This is caused by the high availability of oxygen in the proximity of the vessel which allows the cells to maintain an aerobic metabolism; on the contrary, away from the vessels, the metabolic switch happens and cancer cells with a more anaerobic metabolism can be found (figures 19c, 19d).



(a) $\phi(50, x, y)$.

(b) $\phi(700, x, y)$.



(c) $H(50, x, y)$.

(d) $H(700, x, y)$.

Figure 19: Volume fraction of cancer cells (19a, 19b) and average phenotype distribution (19c, 19d).

5 Conclusions

The present work aims at analyzing and testing a mathematical model describing the evolution in time of cancer cells inside an hypoxic environment and their resistance to low oxygen availability. Different domains and vessels settings were taken into account, compared and studied.

The research shows how crucial it is to use non-local models with a phenotype variable explaining and showing the intra-tumoral variability. In fact, as already mentioned in the results section (cfr. section 4), only the look at the figures representing the volume fraction of cancer cells can already give partial information on what is happening inside the tumor and how cells are migrating and moving over time.

The mono-dimensional scenario numerical simulations have been useful to prove and check the accuracy and precision of the analytical model and of the asymptotic analysis, in particular. The bi-dimensional scenario numerical simulations, instead, have been important to better understand and visualize the phenomena, the different scenarios and setting that can be considered and the fundamental role difference between oxygen and glucose.

Results, in general, confirm that regions with lower oxygen availability are mostly occupied by cancer cells with a higher HIF-1 α level of expression, associated with a metabolism that is mainly anaerobic, i.e. more dangerous because more resistant (phenomena described in [2]). As mentioned multiple times, results prove that the abiotic factor playing a key role on the metabolic switch is, in fact, oxygen; glucose, instead, plays a major role for what concerns the asymptotic volume fraction $\phi^\infty(\mathbf{x})$. Since the presence of abiotic factors is crucial in the analysis, functions describing their availability were given.

It is important to highlight that in order to obtain better and more solid conclusions results should be compared with experimental evidence, not considered in this study, to support the metabolic switch hypothesis and to better understand the reasons behind it.

5.1 On future research

As mentioned previously, the bi-dimensional study could be compared with experimental evidence, followed by a parametric study based on the different kind of vascular cancers.

Another study that can be considered, starting by the current one, could examine the case in which cells behaviour is controlled by two different phenotype or internal variable; in particular, the second variable could describe the resistance of cancer cells with anaerobic metabolism to environments and tissues that are more acid.

For what concerns nutrient factors, time-dependent functions could be considered and applied to the model in order to study how cancer cells react when also levels of nutrients change over time.

Lastly, a model in which the volume fraction of healthy cells is also considered could be made in order to compare the two different volume fractions in the domain to better understand how they distribute, how they interact, how they react to nutrients.

Appendix

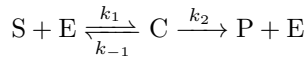
Part I Michaelis-Menten equations

The Michaelis-Menten equation describes the relationship between substrate and enzyme concentrations and the rates of enzyme-catalyzed reactions.

Scientists Leonor Michaelis and Maud Leonora Menten developed this equation/model in the 20th century to explain the difference in the rate of chemical reaction catalyzed by enzymes.

It is an equation that relates reaction velocity to substrate concentration for a system in which a substrate S binds reversibly to an enzyme E to create an enzyme-substrate complex C , which subsequently reacts irreversibly to generate a product P and regenerate the free enzyme E .

This mechanism can be illustrated schematically as follows:



The Michaelis-Menten equation for this system is:

$$v = \frac{V_{max} [S]}{K_M + [S]}$$

In which:

- V_{max} is the *maximum reaction rate*, indicating when all substrate binding sites in an enzyme are full;
- K_M is the Michaelis constant, indicating the concentration of substrate at which the reaction rate is half of its maximum value (V_{max}). The K_M value indicates how well an enzyme is able to perform its activity at different concentrations of its substrate: a lower K_M value indicates better performance.

To better understand when it is appropriate to use Michaelis-Menten equations some assumptions should be made:

1. The initial rate of product formation is proportional to the total concentration of enzyme $[E]_0$ for a given initial concentration of substrate $[S]_0$.
2. In the context of low substrate concentrations, it can be observed that the rate of product formation exhibits a linear relationship with the substrate concentration, denoted as $[S]_0$. This implies that the rate is directly proportional to the substrate concentration.
3. The concentration of the enzyme-substrate complex $[C]$ is assumed as constant. This is referred to as *steady-state approximation*.
4. At a high concentration of substrate, the rate of product formation becomes independent of substrate concentration and reaches a maximum velocity, V_{max} , at which substrate concentration has no effect.

References

- [1] S. Kanwal, Effect of o-glcnacetylation on tamoxifen sensitivity in breast cancer derived mcf-7 cells.
- [2] D. Hanahan, Hallmarks of cancer: New dimensions, *Cancer Discovery* 12 (2022) 31–46. doi: 10.1158/2159-8290.CD-21-1059.
- [3] G. Fiandaca, M. Delitala, T. Lorenzi, A mathematical study of the influence of hypoxia and acidity on the evolutionary dynamics of cancer, *Bulletin of Mathematical Biology* 83. doi: 10.1007/s11538-021-00914-3.
- [4] D. Hanahan, R. Weinberg, The hallmarks of cancer, *Cell* 100 (2000) 57–70. doi:10.1016/S0092-8674(00)81683-9.
- [5] D. Hanahan, R. Weinberg, Hallmarks of cancer: The next generation, *Cell* 144 (2011) 646–74. doi:10.1016/j.cell.2011.02.013.
- [6] B. Reynolds, M. Oli, M. Oli, Eco-oncology: Applying ecological principles to understand and manage cancer, *Ecology and Evolution* 10. doi:10.1002/ece3.6590.
- [7] C. Villa, M. Chaplain, T. Lorenzi, Modeling the emergence of phenotypic heterogeneity in vascularized tumors, *SIAM Journal on Applied Mathematics* 81 (2021) 434–453. doi:10.1137/19M1293971.
- [8] S. Astanin, L. Preziosi, Mathematical modelling of the warburg effect in tumour cords, *Journal of theoretical biology* 258 (2009) 578–90. doi:10.1016/j.jtbi.2009.01.034.
- [9] O. Trédan, C. Galmarini, K. Patel, I. Tannock, Drug resistance and the solid tumor microenvironment, *Journal of the National Cancer Institute* 99 (2007) 1441–54. doi:10.1093/jnci/djm135.
- [10] Y. W. Cho, S. Y. Kim, I. Kwon, I.-S. Kim, Complex adaptive therapeutic strategy (cats) for cancer, *Journal of controlled release : official journal of the Controlled Release Society* 175. doi:10.1016/j.jconrel.2013.12.017.
- [11] U. Martinez-Outschoorn, M. Peiris-Pagès, R. Pestell, F. Sotgia, M. Lisanti, Cancer metabolism: a therapeutic perspective, *Nature reviews. Clinical oncology* 14. doi:10.1038/nrclinonc.2016.60.
- [12] G. Barles, S. Mirrahimi, B. Perthame, Concentration in lotka-volterra parabolic or integral equations: A general convergence result, *Methods and Applications of Analysis* 16. doi: 10.4310/MAA.2009.v16.n3.a4.
- [13] G. Barles, B. Perthame, Concentrations and constrained hamilton-jacobi equations arising in adaptive dynamics, *Contemp. Math.* 439. doi:10.1090/conm/439/08463.
- [14] R. H. Chisholm, T. Lorenzi, A. Lorz, Effects of an advection term in nonlocal lotka–volterra equations, *Communications in mathematical sciences* 14 (4) (2016) 1181–1188.
- [15] T. Lorenzi, B. Perthame, X. Ruan, Invasion fronts and adaptive dynamics in a model for the growth of cell populations with heterogeneous mobility, *European Journal of Applied Mathematics* 33 (4) (2022) 766–783.
- [16] C. Ruhl, Analyze Your Simulation Results with Projection Operators, COMSOL Blog, 2014.
- [17] H. R. Molavian, M. Kohandel, M. Milosevic, S. Sivaloganathan, Fingerprint of cell metabolism in the experimentally observed interstitial ph and po₂ in solid tumors, *Cancer research* 69 (23) (2009) 9141–9147.
- [18] X. Zhao, S. Subramanian, Intrinsic resistance of solid tumors to immune checkpoint blockade therapy, *Cancer research* 77 (4) (2017) 817–822.
- [19] P. J. Mulholland, Surface-subsurface exchange and nutrient spiraling, *Streams and ground waters.* (2000) 149–166.

- [20] S. Spalice, Modellizzazione matematica dell’evoluzione fenotipica di tumori in condizioni di ipossia= mathematical modeling on phenotypic evolution of tumors in hypoxic conditions, Ph.D. thesis, Politecnico di Torino (2021).